

Thermal Diffusivity and Mechanical Properties of Wood

Subjects: [Physics](#), [Condensed Matter](#)

Contributor: Dmitry Golovin

A dependence of Brinell hardness and thermal diffusivity tensor components upon humidity for common pine wood is found. The results of the measurement of Brinell hardness, microhardness, Young's modulus, and main components of thermal diffusivity tensor for three perpendicular cuts are found to be correlated. It is shown that the mechanical properties correlate better with the ratio of longitude to transversal thermal diffusivity coefficients than with the respective individual absolute values. The mechanical characteristics with the highest correlation with the abovementioned ratio are found to be the ratio of Young's moduli in longitude and transversal directions.

thermal diffusivity

dynamic thermal imaging

mechanical properties

Brinell hardness

microhardness

Young's modulus

1. Introduction

It is well known that some mechanical properties of materials can be linked with simple relations due to their similar dependence on material nano- and microstructure. For instance, the hardness H of ductile metals depends upon the yield stress σ_y , as $H \approx 3\sigma_y$, while for hard and superhard metals and alloys, it depends upon the shear modulus G , as $H \approx 0.15 G$ [1]. There is reason to believe that similar relations could link mechanical and thermophysical properties (TPP) of materials belonging to the same type. In particular, thermal conductivity λ and diffusivity a [2][3][4] of wood and other anisotropic composite materials depend on density, porosity, humidity [5][6][7], and specifics of interconnections between microstructural units of the material as hardness, Young's modulus, and strength do [8][9][10]. Once revealed, such relations could allow switching from laborious and material extensively destructive mechanical tests to non-destructive measurements of TPP using express methods, as described in [11][12][13]. Typically, they require around 1 min per measurement and do not demand for cutting samples of any specific geometry. Such approach could be used to estimate relative mechanical properties, sorting, and grading of materials and products made of wood, fiber-reinforced composites etc.

There is a lot of information concerning the mechanical and thermal properties of natural [6][8][10] and modified [14] wood, wood-based layered materials [3][15][16], as well as composites reinforced with artificial [5][9] and natural organic fibers [17][18][19]. For example, it is found that the thermal conductivity of bamboo measured by the classical stationary method along the fibers λ_l exceeds the transversal one λ_n by nearly 2 times [20], and both increase linearly with material density. In [21], the mapping of the thermal conductivity of bamboo cellular structure at the nano- and microscale was carried out by means of scanning thermal microscopy. It provided information about the

relative thermal conductivity of different layers of the cell wall and revealed that the relative thermal conductivity λ^* significantly depended upon the angle between the microfibrils forming the specific layer of cell wall and cell long axis. Thermal conductivity and diffusivity measurements of birch wood in longitude and transverse directions were reported and discussed in [4]. Instances of correlations between thermal conductivity and stiffness of specific layers of the cell wall can be implicitly found in [22].

However, the mechanical and thermal properties are measured in separate tests executed on different samples and are not related to each other, except for several papers that use thermal non-destructive testing to estimate structural damage of wood [23][24][25], defects [26][27], porosity [28], and anisotropy [29][30] of composites and their possible impact on material mechanical properties. In [31], a micromechanical model for the prediction of effective thermal conductivity in two- and three-phase composites is proposed.

2. Relationship between Thermal Diffusivity and Mechanical Properties of Wood

In the first stage of the experiments, the researchers studied Brinell hardness HBW, Young's modulus E (Figure 1a), and the main components a_1 , a_2 , and a_3 of thermal diffusivity tensor (Figure 1b) dependencies in common pine wood on its humidity w . The absolute and relative values of a_1 , a_2 , and a_3 are affected by w differently. The a_1 component displayed significant dependence on w along the fibers, while across the fibers, the dependence of the components a_2 and a_3 upon w was weak, and they were statistically indistinguishable. Hence, it was reasonable to introduce the averaged value $a_n = (a_2 + a_3)/2$ of thermal diffusivity normal to the fibers. The relative values a_i/a_n that characterize thermal diffusivity anisotropy were even more sensitive to humidity change than the absolute ones (Figure 1b).

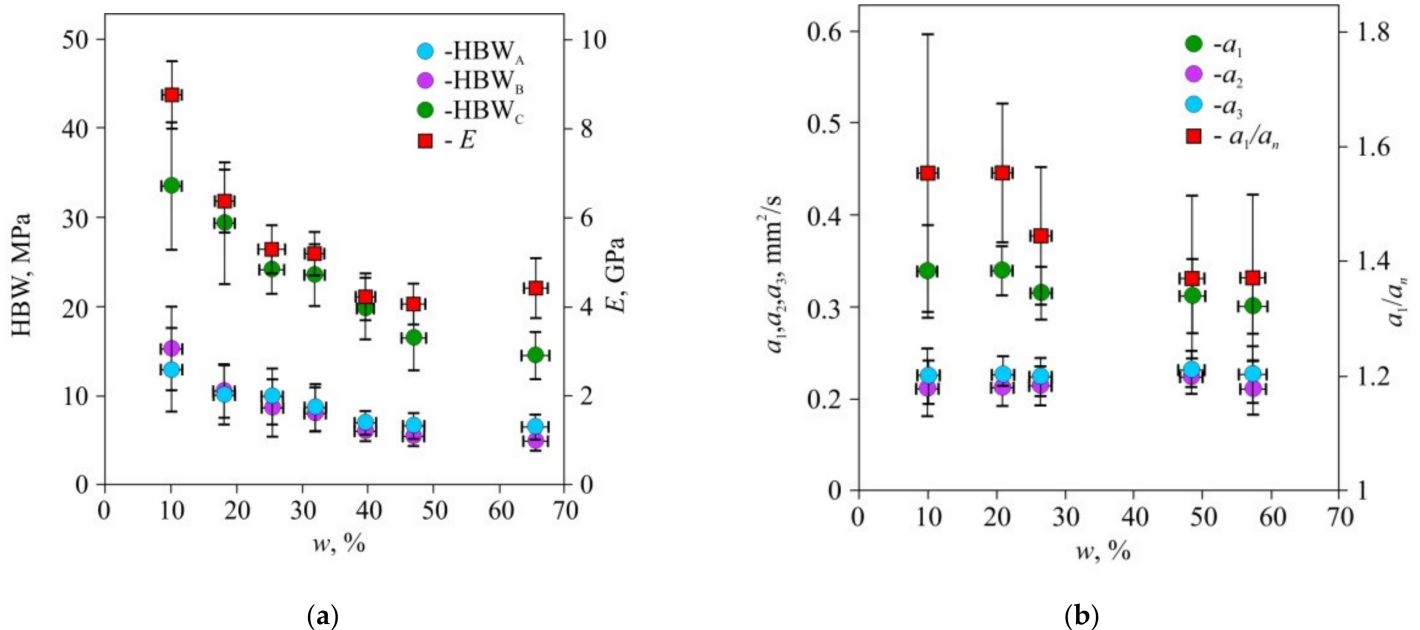


Figure 1. Dependency of Brinell hardness HBW and Young's modulus E (a), thermal diffusivity coefficients a_1 , a_2 , a_3 , and a_1/a_n ratio (b) upon humidity w of pine wood. HBW_A , HBW_B , HBW_C —Brinell hardness on radial, tangential, and cross-fiber cuts. E —Young's modulus across the fibers measured by three-point bending; a_1 , a_2 , a_3 —tangential, radial, and cross-fiber coefficients of thermal diffusivity; $a_n = (a_2 + a_3)/2$.

The values of hardness HBW normalized to the hardness HBW_{10} at $w = 10\%$ for the lateral and radial faces were statistically indistinguishable too (**Figure 2**); therefore, they were approximated as a single set by the following linear function $(HBW/ HBW_{10}) = 1.59(a_1/a_n) - 1.34$ with the coefficient of determination $R^2 = 0.75$. The hardness measured on the face perpendicular to the fibers was found to be independent of tensor a_{ij} components, so that it could be used for method and equipment calibration.

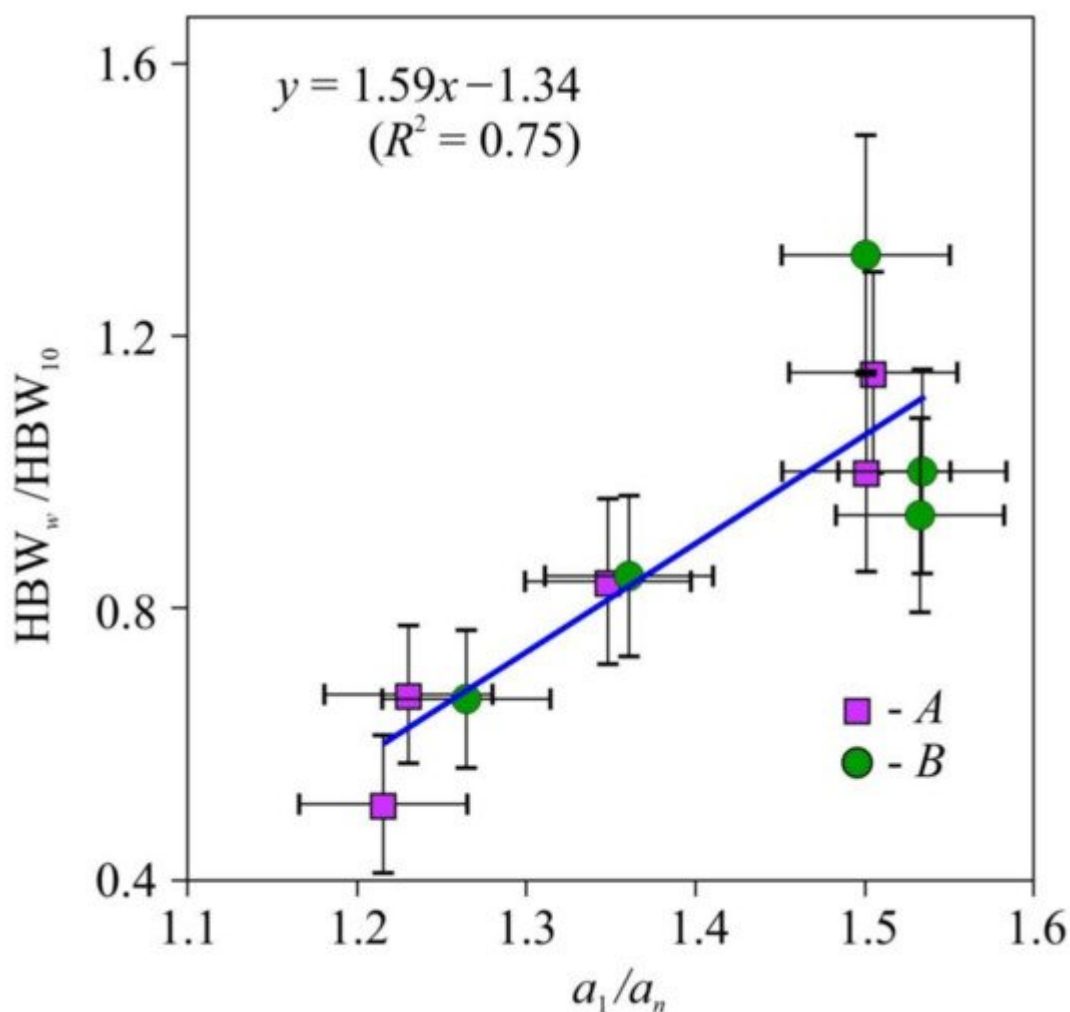


Figure 2. Dependence of the relative macrohardness HBW_w/HBW_{10} of pine wood upon thermal diffusivity anisotropy— a_1/a_n . HBW—Brinell hardness (12.7 mm sphere diameter, 1 mm indentation depth), a_1 , a_n —thermal diffusivity coefficients along and across the fibers. HBW_w/HBW_{10} —HBW values on the faces A and B.

In the second stage of the experiments, microhardness and Young's modulus in early and late wood layers, Brinell hardness HBW, and thermal diffusivity tensor main components were measured in dried wood of all three species

(Figure 3, Figure 4 and Figure 5). Typical P - h curves recorded in NI for the three wood species are shown in Figure 3a, Figure 4a and Figure 5a. Wood of all three species displayed pronounced periodicity of local mechanical properties (Figure 3c, Figure 4c and Figure 5c). Locations of abrupt changes of H_{IT} and E_{IT} coincided with the boundaries of annual growth rings found using an optical method. Changes of H_{IT} and E_{IT} in transition regions between early and late wood in each growth ring were found to be gradual in pine and lime but stepped in oak. H_{IT} and E_{IT} were linked by a linear relation with the same slope $m = 0.017 \pm 0.002$ for all three species (Figure 3b, Figure 4b and Figure 5b). In other words, the ductile ratio $DR = E_{IT}/H_{IT}$ for all studied species appeared to be around 60, which is typical of many wood species. For example, the DR for eucalyptus is between 54 and 68 [32], with an average of 61.

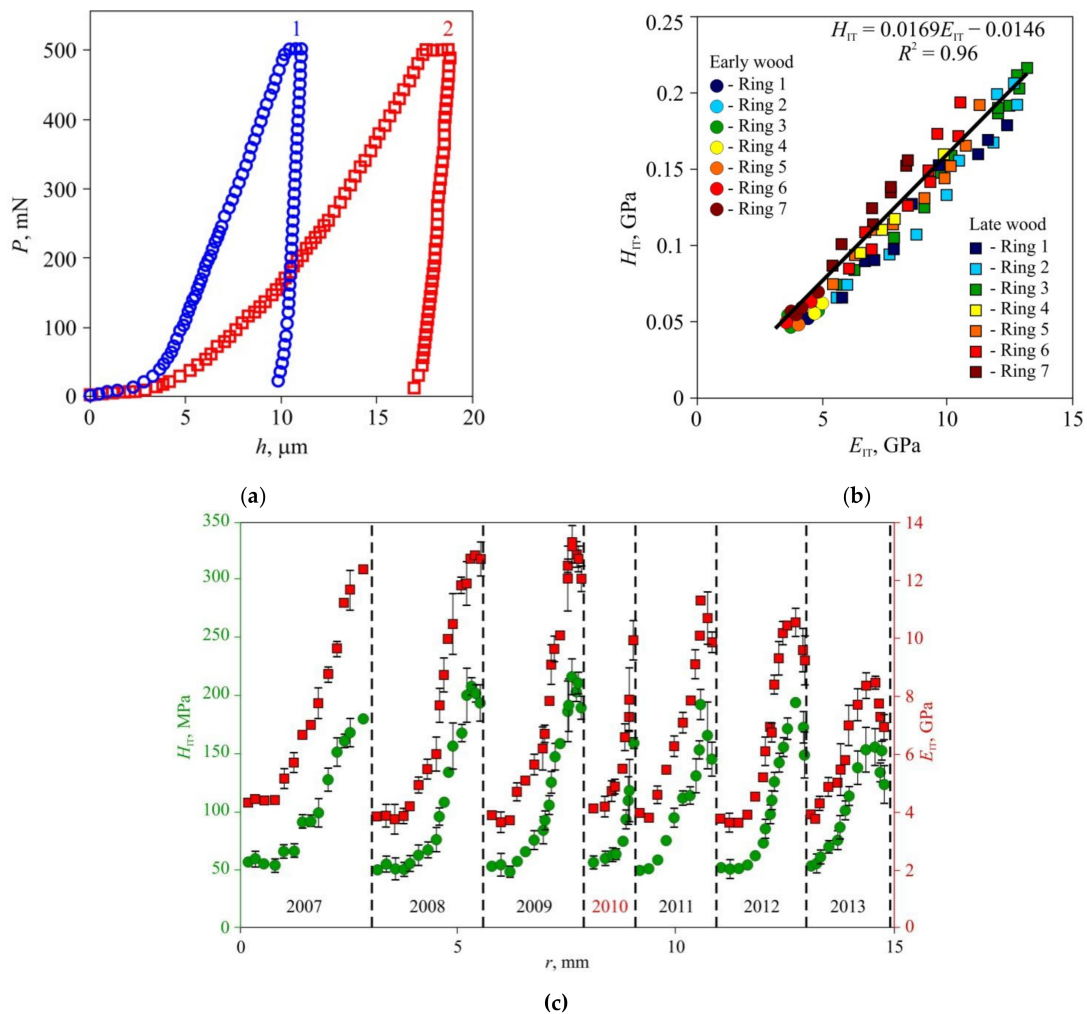


Figure 3. Effective microhardness H_{IT} and Young's modulus E_{IT} in annual rings of pine wood, (a) Typical P - h diagrams for late (1) and early (2) wood; (b) dependence of hardness H_{IT} upon Young's modulus E_{IT} for seven sequential growth rings; (c) spatial distribution of hardness H_{IT} and Young's modulus E_{IT} across sequential growth rings r . The positions of ring boundaries are shown by dashed lines. The corresponding years for the growth rings are shown below the data points. An extraordinary dry year is indicated in red.

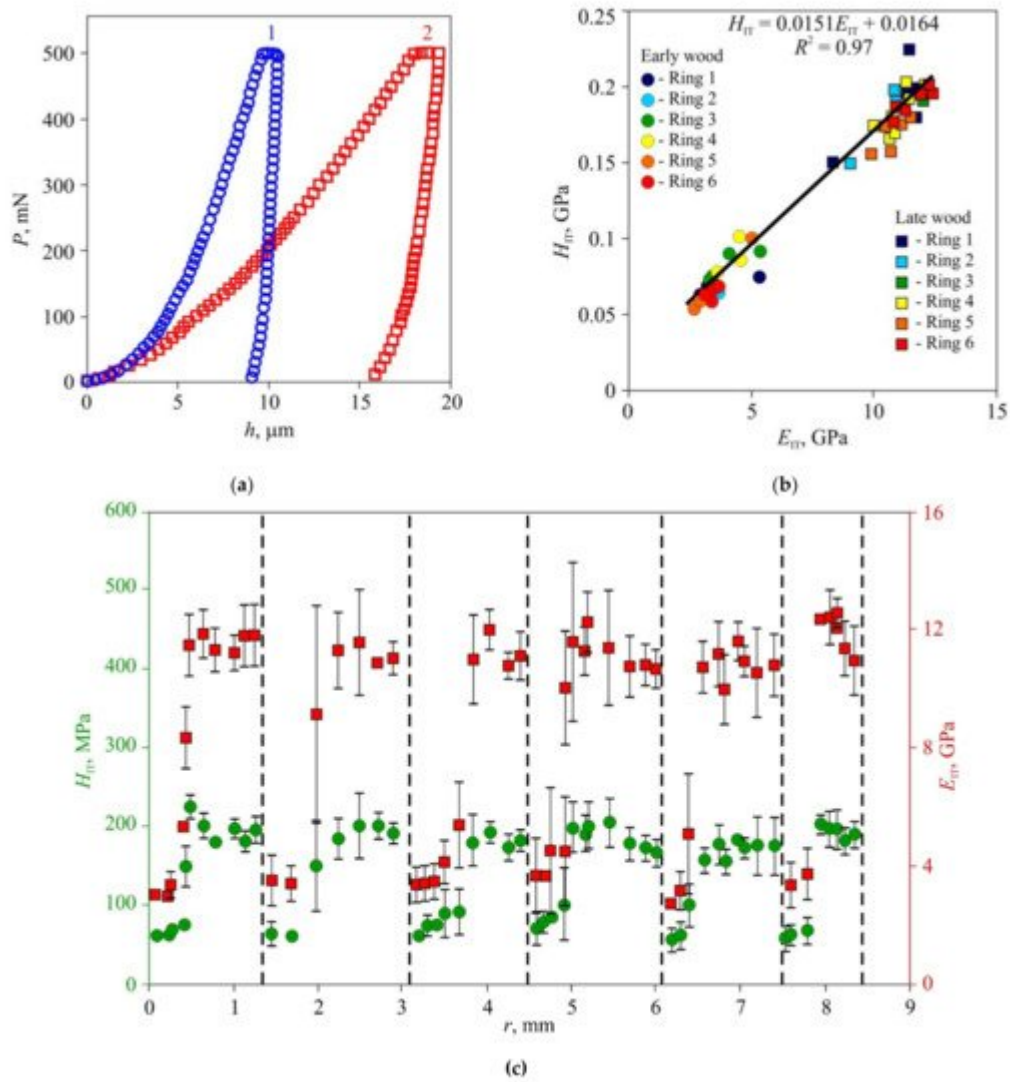


Figure 4. Effective microhardness H_{IT} and Young's modulus E_{IT} in annual rings of oak wood, (a) Typical P - h diagrams for late (1) and early (2) wood; (b) dependence of hardness H_{IT} upon Young modulus E_{IT} for seven sequential growth rings; (c) spatial distribution of hardness H_{IT} and Young modulus E_{IT} across sequential growth rings r . The positions of ring boundaries are shown by dashed lines.

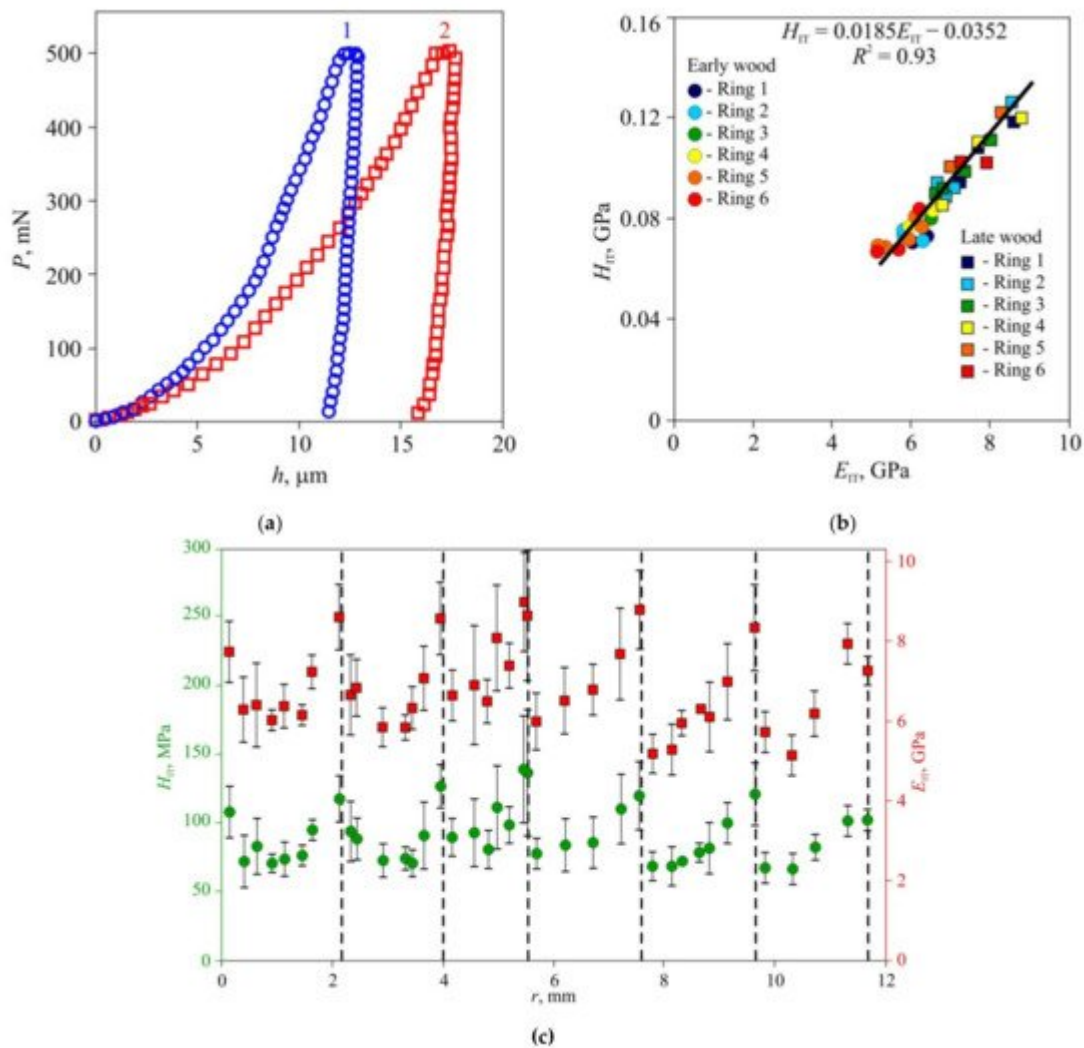


Figure 5. Effective microhardness H_{IT} and Young's modulus E_{IT} in annual rings of lime wood, (a) Typical $P-h$ diagrams for late (1) and early (2) wood; (b) dependence of hardness H_{IT} upon Young's modulus E_{IT} for seven sequential growth rings; (c) spatial distribution of hardness H_{IT} and Young's modulus E_{IT} across sequential growth rings r . The positions of ring boundaries are shown by dashed lines.

The values of H_{IT} and E_{IT} of the EW layer differed only slightly (within 10–15%) both within each ring and for different rings, despite the growth conditions differing significantly. For instance, in 2010, there was a severe drought, so that the width of the growth ring in pine wood was less than half its normal value; however, there was no discernible effect on H_{IT} and E_{IT} of EW. The lateral sizes of cells corresponding to different years had no visible difference too, but the wall thickness did differ. Therefore, the variation of the annual growth ring width was attributed to the different number of cells in the layer, while the size and mechanical properties of each cell remained almost the same. Effective hardness and Young's modulus of the LW layers were several times higher than those of the EW layers due to higher cell wall thickness and lower lumen area.

In the third stage of the experiments, tensor a_{ij} components and Brinell hardness HBW were measured for the three wood species. Effective values of H_{IT} , E_{IT} , HBW, and thermal diffusivity anisotropy are presented in **Table 1**. As can be seen, all mechanical characteristics correlated with the ratio of the main components of the thermal

diffusivity tensor, and for E , such correlation was about three times stronger than for H_{IT} or HBW (Figure 6). It should be mentioned that the mechanical and thermal properties were correlated in all three studied species with significantly different microstructures.

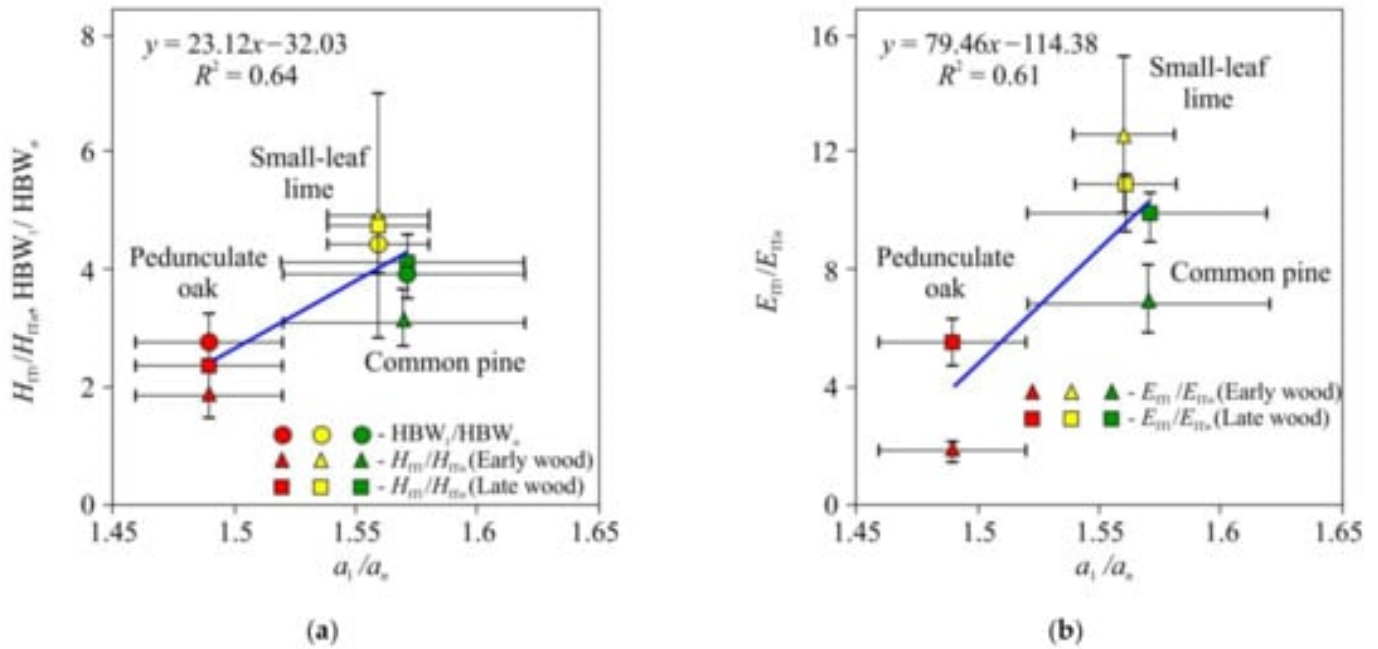


Figure 6. Dependencies of the physico-mechanical properties H_{IT1}/H_{ITn} , HBW_1/HBW_n (a), and E_{IT1}/E_{ITn} (b) upon thermo-physical characteristics (a_1/a_n) for common pine, pedunculate oak, and small-leaf lime.

Table 1. Measured micro-/macromechanical and thermal physical properties of wood of the three studied species.

Type of Wood	Micromechanical Properties (Obtained by Nanoindentation with $P_{max} = 500$ mN)						Macromechanical Properties			TPP
	E_{IT1} , GPa	E_{ITn} , GPa	E_{IT1}/E_{ITn}	H_{IT1} , MPa	H_{ITn} , MPa	H_{IT1}/H_{ITn}	HBW_1 , MPa	HBW_n , MPa	HBW_1/HBW_n	
Common pine (<i>Pinus sylvestris</i> L.)										
Early wood	4.39 ± 0.04	0.44 ± 0.04	10 ± 1	57 ± 2	14 ± 1	4.0 ± 0.5	42 ± 2	11 ± 1	3.9 ± 0.7	1.57 ± 0.05
Late wood	12.4 ± 0.7	1.8 ± 0.2	7 ± 1	180 ± 10	58 ± 4	3.1 ± 0.4				
Pedunculate oak (<i>Quercus robur</i> L.)										
Early wood	3.1 ± 0.2	1.7 ± 0.2	1.9 ± 0.3	64 ± 3	34 ± 5	1.9 ± 0.4	67 ± 4	24 ± 3	2.8 ± 0.5	1.49 ± 0.03
Late wood	11.1 ± 0.8	2.0 ± 0.2	5.6 ± 0.8	190 ± 20	80 ± 8	2.4 ± 0.4				

Type of Wood	Micromechanical Properties (Obtained by Nanoindentation with $P_{\max} = 500$ mN)						Macromechanical Properties			TPP
	E_{IT1} , GPa	E_{ITn} , GPa	E_{IT1}/E_{ITn}	H_{IT1} , MPa	H_{ITn} , MPa	H_{IT1}/H_{ITn}	HBW_1 , MPa	HBW_n , MPa	HBW_1/HBW_n	a_1/a_n
Small-leaf Lime (<i>Tilia cordata</i> Mill.)										
Early wood	6.7 ± 0.1	0.61 ± 0.08	11 ± 2	75 ± 4	16 ± 3	5 ± 1	39.4 \pm 1.5	8.9 \pm 0.6	4.4 \pm 0.5	1.56 \pm 0.02
Late wood	8.6 ± 0.8	0.68 ± 0.08	13 ± 3	120 ± 20	24 ± 7	5 ± 2				

1. Hsueh, C.-H.; Schmauder, S.; Chen, C.-S.; Chawla, K.K.; Chawla, N.; Chen, W.; Kagawa, Y. (Eds.) Handbook of Mechanics of Materials; Springer Nature Singapore Pte Ltd.: Gateway East, Singapore, 2019; 2464p.
2. Krištak, L.; Igaz, R.; Ružiak, I. Applying the EDPS Method to the Research into Thermophysical Properties of Solid Wood of Coniferous Trees. Adv. Mater. Sci. Eng. 2019, 2019, 2303720.
3. Kristak, L.; Ruziak, I.; Tudor, E.M.; Barbu, M.C.; Kain, G.; Reh, R. Thermophysical Properties of Larch Bark Composite Panels. Polymers 2021, 13, 2287.
4. Suleiman, B.; Larfeldt, J.; Leckner, B.; Gustavsson, M. Thermal conductivity and diffusivity of wood. Wood Sci. Technol. 1999, 33, 465–473.
5. Rajak, D.K.; Pagar, D.D.; Menezes, P.L.; Linul, E. Fiber-reinforced polymer composites: Manufacturing, properties, and applications. Polymers 2019, 11, 1667.
6. Hassani, N.J.M. Physical and Mechanical Properties of Wood. 2018. Available online: <https://forestrypedia.com/physical-and-mechanical-properties-of-wood/> (accessed on 12 August 2021).
7. Chen, C.; Kuang, Y.; Zhu, S.; Burgert, I.; Keplinger, T.; Gong, A.; Li, T.; Berglund, L.; Eichhorn, S.J.L.; Hu, L. Structure–property–function relationships of natural and engineered wood. Nat. Rev. Mater. 2020, 5, 642–666.
8. Ross, R. Forest Products Laboratory. In Wood handbook—Wood as an Engineering Material; General Technical Report FPL-GTR-282; U.S. Department of Agriculture, Forest Service, Forest Products Laboratory: Madison, WI, USA, 2021; 543p.
9. Luan, C.; Movva, S.; Wang, K.; Yao, X.; Zhang, C.; Wang, B. Towards next-generation fiber-reinforced polymer composites: A perspective on multifunctionality. Funct. Compos. Struct. 2019, 1, 042002.
10. Senalik, C.A.; Farber, B. Mechanical Properties of Wood. Ch. 5. In Wood Handbook—Wood as an Engineering Material; General Technical Report FPL-GTR-282; U.S. Department of Agriculture,

- Forest Service, Forest Products Laboratory: Madison, WI, USA, 2021; pp. 5.1–5.46.
11. Golovin, D.Y.; Divin, A.G.; Samodurov, A.A.; Tyurin, A.I.; Golovin, Y.I. Temperature diffusivity measurement and nondestructive testing requiring no extensive sample preparation and using stepwise point heating and IR thermography. In *Failure Analysis*; Huang, Z.-M., Hemed, S., Eds.; InTech: London, UK, 2019; pp. 124–160.
 12. Golovin, D.Y.; Samodurov, A.A.; Tyurin, A.I.; Golovin, Y.I.; Divin, A.G. A new rapid method of determining the thermal diffusivity of materials and finished articles. *J. Eng. Phys. Thermophys.* 2020, 93, 234–240.
 13. Golovin, D.Y.; Tyurin, A.I.; Samodurov, A.A.; Divin, A.G.; Golovin, Y.I. Dinamicheskiye termograficheskiye metody nerazrushayushchego ekspress-kontrolya (Dynamic Thermographic Methods of NDT); Technosfera: Moscow, Russia, 2019; 214p. (In Russian)
 14. Thybring, E.E.; Fredriksson, M. Wood modification as a tool to understand moisture in wood. *Forests* 2021, 12, 372.
 15. Edgars, L.; Kaspars, Z.; Kaspars, K. Structural performance of wood based sandwich panels in four point bending. *Procedia Eng.* 2017, 172, 628–633.
 16. Hao, J.; Wu, X.; Oporto, G.; Liu, W.; Wang, J. Structural analysis and strength-to-weight optimization of wood-based sandwich composite with honeycomb core under three-point flexural test. *Eur. J. Wood Prod.* 2020, 78, 1195–1207.
 17. Pickering, K.L.; Efendy, M.G.A.; Le, T.M. A review of recent developments in natural fibre composites and their mechanical performance. *Compos.-A Appl. Sci. Manuf.* 2016, 83, 98–112.
 18. Syduzzaman, M.; Al Faruque, M.A.; Bilisik, K.; Naebe, M. Plant-based natural fibre reinforced composites: A review on fabrication, properties and applications. *Coatings* 2020, 10, 973.
 19. Huang, X.; Yang, L.; Meng, L.; Lu, J. Mechanical and thermal properties of cellulose nanocrystals from jute fibers reinforced epoxy composites. *J. Text. Inst.* 2021, 1–5.
 20. Shah, D.U.; Bock, M.C.D.; Mulligan, H.H.; Ramage, M.H. Thermal conductivity of engineered bamboo composites. *J. Mater. Sci.* 2016, 51, 2991–3002.
 21. Shah, D.U.; Konnerth, J.; Ramage, M.H.; Gusenbauer, C. Mapping thermal conductivity across bamboo cell walls with scanning thermal microscopy. *Sci. Rep.* 2019, 9, 16667.
 22. Toumpanaki, E.; Shah, D.U.; Eichhorn, S.J. Beyond what meets the eye: Imaging and imagining wood mechanical–structural properties. *Adv. Mater.* 2021, 33, 2001613.
 23. Catena, A. Thermography reveals hidden tree decay. *Arboric. J.* 2003, 27, 27–42.
 24. Catena, A.; Catena, G. Overview of thermal imaging for tree assessment. *Arboric. J.* 2012, 30, 259–270.

25. Vidal, D.; Pitarma, R. Infrared thermography applied to tree health assessment: A review. *Agriculture* 2019, 9, 156.
26. Palumbo, D.; Cavallo, P.; Galietti, U. An investigation of the stepped thermography technique for defects evaluation in GFRP materials. *NDT E Int.* 2019, 102, 254–263.
27. Addepalli, S.; Zhao, Y.; Roy, R.; Galhenege, W.; Colle, M.; Yu, J.; Ucur, A. Nondestructive evaluation of localized heat damage occurring in carbon composites using thermography and thermal diffusivity measurement. *Measurement* 2019, 131, 706–713.
28. Meola, C.; Toscano, C. Flash thermography to evaluate porosity in carbon fiber reinforced polymer (CFRPs). *Materials* 2014, 7, 1483–1501.
29. Guo, J.; Gao, X.; Toma, E.; Netzelmann, U. Anisotropy in carbon fiber reinforced polymer (CFRP) and its effect on induction thermography. *NDT E Int.* 2017, 91, 1–8.
30. Adamczyk, W.; Ostrowski, Z.; Ryfa, A. Development of a non-destructive technique for measuring thermal conductivity of material with small anisotropy based on application of the reduced order technique. *Measurement* 2020, 165, 108078.
31. Lages, E.N.; Marques, S.P.C. Prediction of effective thermal conductivity of multiphase composites with periodic microstructures using an expanded micromechanical model. *Int. J. Therm. Sci.* 2022, 171, 107226.
32. Carrillo-Varela, I.; Valenzuela, P.; Gasitua, W.; Mendoca, R.T. An evaluation of fiber biometry and nanomechanical properties of different eucalyptus species. *Bioresources* 2019, 14, 6433.

Retrieved from <https://www.encyclopedia.pub/entry/history/show/46514>